



ELSEVIER

Available online at [www.sciencedirect.com](http://www.sciencedirect.com)

SCIENCE @ DIRECT®

Earth and Planetary Science Letters 228 (2004) 299–310

EPSL

[www.elsevier.com/locate/epsl](http://www.elsevier.com/locate/epsl)

# Miocene faulting at plate tectonic velocity in the Himalaya of central Nepal

Matthew J. Kohn<sup>a,\*</sup>, Mark S. Wieland<sup>a</sup>, Christopher D. Parkinson<sup>b</sup>, Bishal N. Upreti<sup>c</sup>

<sup>a</sup>Department of Geological Sciences, University of South Carolina, Columbia, SC 29208, United States

<sup>b</sup>Department of Geology and Geophysics, University of New Orleans, New Orleans, LA 70148, United States

<sup>c</sup>Department of Geology, Tribhuvan University, Tri-Chandra Campus, Ghantaghar, Kathmandu, Nepal, United States

Received 7 April 2004; received in revised form 27 September 2004; accepted 11 October 2004

Available online 11 November 2004

Editor: K. Farley

## Abstract

Combination of geochemical zoning in metamorphic garnet and monazite plus in situ Th–Pb isotopic dating of monazite yields  $P$ – $T$  conditions, ages and convergence rates for the Main Central Thrust (MCT) and affiliated faults in central Nepal. Inferred rates were  $1.5 \pm 0.9$  cm/yr (Langtang Thrust,  $\sim 19$  Ma),  $2.2 \pm 0.7$  cm/yr (Main Central Thrust,  $\sim 15$  Ma) and  $7 \pm 3$  cm/yr (Ramgarh Thrust,  $\sim 10$  Ma). The lower values are similar to modern convergence rates across the Himalaya, but the Ramgarh Thrust may have briefly absorbed all Indo–Asian convergence at  $\sim 10$  Ma, when foreland and marine sedimentation rates markedly increased, and at least one major strike slip fault in Tibet experienced a hiatus in movement. Variable rates of convergence across the Himalaya on Myr timescales imply Myr variations in strain rates throughout all components of the Indo–Asian orogen.

© 2004 Elsevier B.V. All rights reserved.

**Keywords:** Himalaya; geochronology; monazite; metamorphism; melting

## 1. Introduction

Shortening across the Himalaya has played a major role in accommodating Indo–Asian convergence. At least 650 km of convergence between India and Asia was taken up across the Himalaya

[1], and today shortening in the Himalaya accounts for roughly 40% of the 5 cm/yr Indo–Asian convergence rate [2,3]. Past accommodation rates are poorly known, yet crucial for understanding strain partitioning in this classic orogen. For the Main Central Thrust (MCT) and closely affiliated Ramgarh Thrust, previous studies in Nepal have inferred disparate times of activity at ca. 20–22 Ma [4,5],  $\sim 8$  Ma [6,7] or progressive in-sequence thrusting sometime between 20 and 8 Ma [1,8]. However, clear identification of faults, their ages,

\* Corresponding author. Tel.: +1 803 777 5565; fax: +1 803 777 6610.

E-mail address: [mjk@geol.sc.edu](mailto:mjk@geol.sc.edu) (M.J. Kohn).

and displacement amounts and rates is convoluted in central Nepal. Here, we show that chemical zoning in garnet and monazite (a light-rare-earth-element phosphate that contains a large amount of Th), together with in situ  $^{232}\text{Th}$ – $^{208}\text{Pb}$  dating of monazite clearly delineate discrete thrust packages, and the timing of thrust movement in the Langtang region of central Nepal (Figs. 1 and 2). These data define timing and pressure–temperature conditions of thrust sheet emplacement, and most importantly rates of thrust movement and convergence.

## 2. Field area

The Langtang region was chosen for study because it exhibits a classic Himalayan transition from low-grade to high-grade metamorphic rocks structurally upward. Previous workers there [9–12]

used lithologic distributions to infer between 2 and 11 faults near the contact between the Greater and Lesser Himalayan Sequences (GHS and LHS). Our remapping (Fig. 1) does generally confirm lithologic distributions, but not the presence of all inferred faults. Neodymium isotopes (summarized in [12]) define the GHS-LHS boundary near a quartzite at the base of GHS1. The MCT is commonly assigned to this boundary, although penetrative deformation clearly occurs both above and below structurally. Both Pearson's [12] and our observations imply that unit LHS4 is a package of lower Lesser Himalayan rocks, bounded above and below by the major Main Central and Ramgarh Thrusts. By implication, structurally lower rocks of the LHS are part of the Lesser Himalayan duplex [1,8]. The N–S orientation of the MCT in the Langtang region is somewhat unusual, but the consistency of foliation orientations across lithologic boundaries suggests

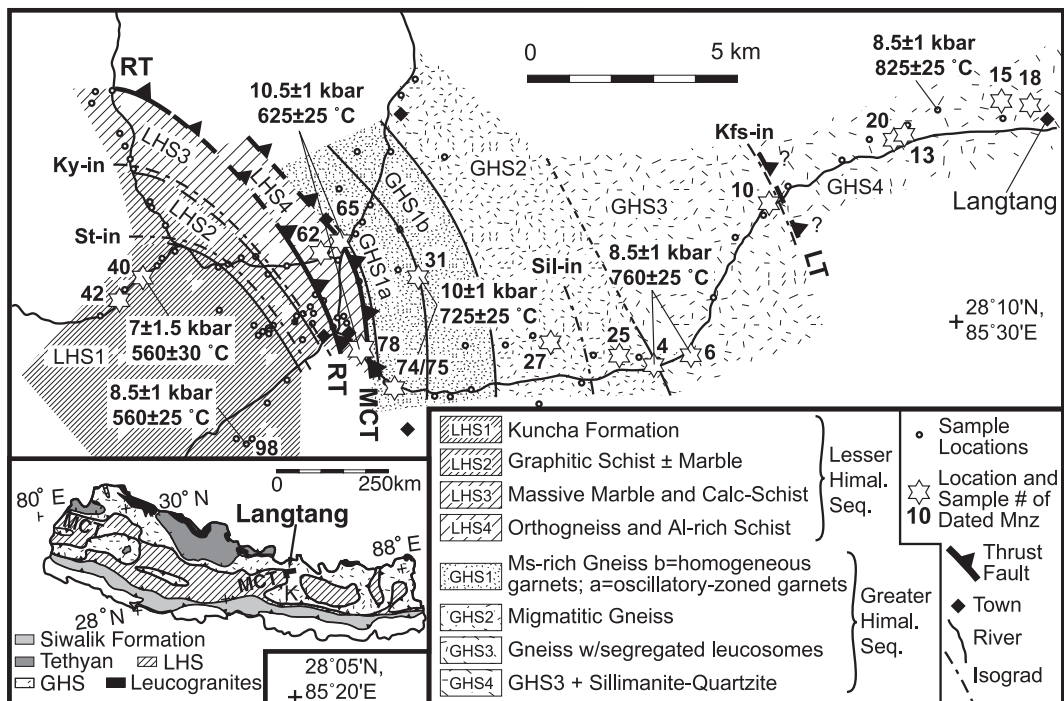


Fig. 1. Geologic map of Langtang region, showing sample locations, lithologic units and inferred thrusts. Units GHS1 through GHS4 correspond with Formation 1 [33] of the Greater Himalayan Sequence. LHS2 corresponds with the Nourpul Formation, Dhading Dolomite and Benighat Slate; LHS3 corresponds with the Malekhu Limestone and overlying calcareous schists; LHS4 corresponds with the Ulleri augen gneiss and associated aluminous schists. Units LHS1 through LHS3 are in stratigraphic order, whereas LHS4 is a structural repetition, identified in western Nepal as the Ramgarh Thrust sheet [1]. LT, MCT and RT are the Langtang, Main Central and Ramgarh Thrusts, respectively. Inset shows major faults and location of Langtang area.

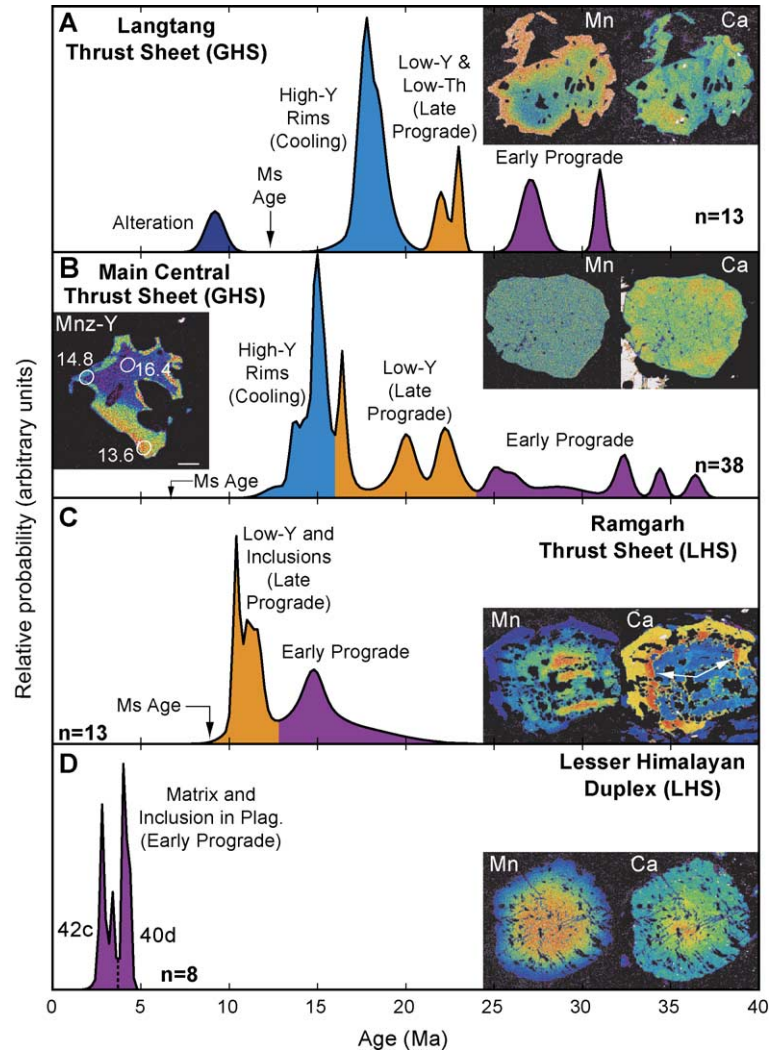


Fig. 2. Probability distributions of monazite ages, distinguished according to monazite chemistry. Insets show garnet and monazite zoning patterns, with “hot” vs. “cold” colors denoting high vs. low concentrations. Arrows show published  $^{40}\text{Ar}/^{39}\text{Ar}$  ages from same structural levels. GHS rocks contain compositionally identifiable prograde vs. retrograde monazite domains, whereas LHS rocks only contain prograde monazite. (A) Highest structural level (Langtang Thrust sheet). (B) Main Central Thrust sheet. (C) Ramgarh Thrust sheet. (D) Lesser Himalayan duplex.

the strike results simply from late-stage warping [12], possibly associated with an underlying lateral ramp [10].

### 3. Methods

Electron microprobe data (Table 1) were collected by using the fully automated Cameca SX-50 housed in the Electron Microscopy Center, University of

South Carolina. These data were used to estimate pressure–temperature conditions (Table 2), to guide chronologic analysis of monazite (Table 3) and to characterize compositional differences that could be linked to petrologic and structural discontinuities. For quantitative analyses of silicates, operating conditions were 15 kV accelerating voltage, 20 s count time, 20 nA cup current and a spot size of 2  $\mu\text{m}$  for garnet, and 5  $\mu\text{m}$  for micas and feldspar. Natural minerals were used as standards. For

Table 1  
Silicate compositions from schists and gneisses, Langtang region, Nepal

Sample	40	98	65	78	75	31	4	6	14
<i>Muscovite</i>									
Si	3.100	3.066	3.158	3.096	3.086	3.065	3.112	3.038	3.082
Ti	0.009	0.016	0.030	0.017	0.038	0.034	0.016	0.041	0.026
Al	2.759	2.701	2.644	2.779	2.705	2.775	2.586	2.796	2.775
Mg	0.059	0.149	0.093	0.085	0.089	0.073	0.094	0.064	0.061
Ca	0.000	0.000	0.000	0.003	0.000	0.000	0.000	0.001	0.000
Mn	0.000	0.002	0.000	0.001	0.002	0.002	0.003	0.001	0.001
Fe	0.089	0.175	0.083	0.043	0.109	0.082	0.105	0.081	0.073
Na	0.215	0.107	0.137	0.235	0.238	0.109	0.162	0.079	0.092
K	0.774	0.811	0.829	0.717	0.749	0.858	0.807	0.922	0.885
Total (wt.%)	95.502	94.295	94.502	94.760	95.330	94.413	94.682	94.638	95.335
Fe/(Fe+Mg)	0.601	0.540	0.472	0.336	0.551	0.529	0.528	0.559	0.545
<i>Biotite</i>									
Si	2.715	2.721	2.752	2.749	2.775	2.690	2.726	2.677	2.659
Ti	0.106	0.081	0.149	0.083	0.087	0.139	0.091	0.214	0.160
Al	1.709	1.705	1.621	1.683	1.628	1.675	1.642	1.662	1.755
Mg	0.905	0.965	0.519	1.422	1.288	0.864	0.952	0.814	0.828
Ca	0.000	0.002	0.000	0.002	0.006	0.000	0.001	0.001	0.004
Mn	0.006	0.008	0.018	0.001	0.003	0.011	0.005	0.01	0.009
Fe	1.407	1.403	1.761	0.95	1.073	1.515	1.389	1.435	1.414
Na	0.043	0.032	0.015	0.042	0.036	0.021	0.035	0.03	0.039
K	0.906	0.889	0.928	0.832	0.889	0.857	0.882	0.905	0.912
Total (wt.%)	95.92	94.740	95.321	95.02	95.97	95.03	95.45	96.01	96.17
Fe/(Fe+Mg)	0.609	0.592	0.772	0.401	0.454	0.637	0.593	0.638	0.631
<i>Garnet</i>									
Si	2.988	2.976	3.012	2.954	2.984	2.998	2.915	2.983	2.981
Ti	0.002	0.003	0.004	0.002	0.000	0.000	0.001	0.001	0.000
Al	1.996	2.023	1.919	2.013	2.010	1.994	1.990	1.999	2.011
Mg	0.240	0.218	0.077	0.565	0.594	0.304	0.430	0.319	0.409
Fe	2.522	2.344	2.091	2.316	2.150	2.362	2.414	2.244	2.357
Mn	0.100	0.066	0.110	0.016	0.117	0.126	0.175	0.327	0.162
Ca	0.160	0.376	0.809	0.170	0.156	0.220	0.116	0.140	0.093
Total (wt.%)	101.490	99.489	99.514	100.709	101.114	101.785	99.299	100.854	100.386
Fe/(Fe+Mg)	0.913	0.915	0.964	0.804	0.784	0.886	0.849	0.876	0.852
Prp	0.079	0.073	0.025	0.184	0.197	0.101	0.137	0.105	0.135
Alm	0.835	0.780	0.677	0.755	0.713	0.784	0.770	0.741	0.780
Sps	0.033	0.022	0.036	0.005	0.039	0.042	0.056	0.108	0.054
Grs	0.053	0.125	0.262	0.055	0.052	0.073	0.037	0.046	0.031

Compositions are normalized to an anhydrous oxygen basis of: 12 (garnet), 11 (micas) and 14 (chlorite). Iron calculated assuming all Fe<sup>2+</sup>. Rim plagioclase compositions are: An<sub>12</sub> (40), An<sub>20</sub> (98), An<sub>15</sub> (65), An<sub>23</sub> (78), An<sub>19</sub> (75), An<sub>19</sub> (31), An<sub>16</sub> (4), An<sub>24</sub> (6), An<sub>20</sub> (14).

quantitative analyses of monazite, operating conditions were 20 kV accelerating voltage, 20 nA cup current and a spot size of 5  $\mu\text{m}$ . Synthetic phosphates and a natural apatite were used as standards. For X-ray maps, we used an accelerating voltage of 15 kV, a cup current of 200 nA and time per pixel of 30 ms, with a pixel resolution dependent on crystal size—typically 1–5  $\mu\text{m}$ .

Ion microprobe Th–Pb analyses of monazite grains (Table 3) were collected in situ with the Cameca IMS 1270 housed at the Department of Earth and Space Sciences, University of California–Los Angeles. Monazite grains were first identified in thin section and mapped for Th, U, Y and Si distributions by electron microprobe. Individual grains were then drilled out using either a 1/4- or

Table 2  
Pressure–temperature conditions from schists and gneisses, Langtang region, Nepal

Sample	40	98	65	78	75	31	4	6	14
<i>Pressure–temperature conditions</i>									
<i>P</i> (kbar)	7	8.5	10.5	10.5	10	10.5	9	8	8.5
<i>T</i> (°C)	560	560	600	625	700	725	775	750	825
Zone	Gr	Gr	Ky	Ky	Ky	Ky	Sil	Sil	Sil-Kfs

Temperatures calculated by using the garnet–biotite thermometer [34,35]. Alternative recent calibrations (e.g., [36]) do not yield significantly different results. Pressures calculated from garnet–plagioclase–muscovite–biotite, garnet–plagioclase–kyanite/sillimanite–quartz and garnet–plagioclase–biotite–quartz barometry [37,38]. Retrieved *P–T* conditions are consistent with phase equilibria, specifically the expected stability fields for sub-stauroliite-, kyanite- and sillimanite-grade rocks (e.g., [39]), and the *P–T* conditions of muscovite dehydration-melting (e.g., [40]). The occurrence of migmatitic rocks in both the kyanite and sillimanite zones, plus the occurrence of late-stage muscovite and quartz after sillimanite indicates minimum temperatures of 700 °C for samples 4, 6 and 14.

1/8-in. diamond drill corer. Most crystals were relatively large, chemically complex matrix grains, but inclusions were also analyzed (Table 3). Grains were mounted together with the UCLA 554 monazite standard in 1-in. epoxy rounds. Operating conditions are essentially as described previously [13], and for this study involved a primary beam current of 6–12 nA, a spot size of ~10–30 μm, energy offsets for  $^{232}\text{Th}^+$  and  $\text{ThO}_2^+$  of +10 to 15 and –8 to –13 eV, respectively, and a MRP of ~5000, which was sufficient to discriminate peak interferences. Total analysis time per spot was ~15 min. Common Pb corrections assumed  $^{208}\text{Pb}/^{204}\text{Pb}=38.6$  [14], but alternative assumptions do not yield significantly different ages (Table 3). Reported age uncertainties reflect counting statistics and the reproducibility of the  $^{264}\text{ThO}_2^{+}/^{232}\text{Th}^+$  vs.  $^{208}\text{Pb}^{*+}/^{232}\text{Th}^+$  calibration curve, as determined from multiple spots on the standard.

#### 4. Mineral chemistry

Garnet chemistry is one key component of our tectonic interpretation (Fig. 2). In structurally low units, garnets ubiquitously exhibit growth zoning, in which Mn decreases systematically from core to rim. However, in unit LHS4, garnets also exhibit Ca-poor cores overgrown by Ca-rich rims, indicating a differ-

ent metamorphic history. This distinction is consistent with our mapping (Fig. 1), which implies that LHS4 is bounded below by the Ramgarh Thrust. In structurally higher units (GHS1–4), garnets are diffusively modified and resorbed, typically yielding flat or increasing Mn from core to rim. The transition from preserved garnet growth zoning to strong diffusional modification co-occurs with the Nd isotope boundary, and thus also defines the GHS–LHS contact (the MCT). Garnet and matrix mineral compositions imply that temperatures systematically increase structurally upward, with higher pressures in units LHS4 and GHS1 (Tables 1 and 2; Fig. 1).

A second key component of this study is the chemistry and age of monazite (Table 3, Fig. 2). Monazite’s extremely low initial Pb content and high Pb retentivity make it an excellent mineral for U–Th–Pb geochronology [15]. In meta-sedimentary rocks, monazite growth and chemistry are directly linked to silicate mineral formation [16,17]. The following summary and interpretation of Y and Th trends is based on previous study of pelitic schists [16–18]. In rocks that lack xenotime, the majority of Y is hosted by garnet and monazite. Consequently, as garnet grows and sequesters Y during prograde metamorphism, the Y content of monazite must decrease, at least up until melting. Monazite growth contributes to this effect, and also fractionates Th, causing it to decrease with increasing grade. The Y trend is evident in unit LHS4, where lower-Y monazite grains generally yield younger ages (Table 3). If melting occurs, garnet continues to grow, but monazite largely dissolves into the melt, so it will not preserve this event chemically. However, upon cooling and melt crystallization, new monazite grows, either as new grains or as mantles on old (low-Y, low-Th) monazite cores. Although Th trends during melt crystallization are not well understood, Y content of retrograde monazite should be high, both because garnet dissolves as the melt crystallizes, and because monazite strongly partitions Y [17]. This trend is evident in GHS units, where low-Y cores are overgrown by chronologically younger, high-Y rims (Fig. 2B, Table 3). Thus, Y and Th zoning maps plus in situ age determinations permit specific areas in monazite grains to be linked with the heating vs. cooling portion of a rock’s history. In all rocks, increasingly low-Y and -Th domains generally reflect increasingly high subsolidus temperatures. In migma-

Table 3  
Monazite ages and compositions

Sample	Grain	Age $\pm 2\sigma$	% radio	$X_Y, X_{Th}$	Comment
18	14	17.7 $\pm$ 0.9	92	0.059, 0.041	High-Y rim
	5	21.9 $\pm$ 0.7	91	0.009, 0.080	Low-Y
15	11	9.2 $\pm$ 1.1	27	0.013, 0.038	Alteration Mnz
	11	17.5 $\pm$ 2.3	59	0.067, 0.051	High-Y
	11	NA	NA	0.026, 0.051	Low-Y
	6	18.4 $\pm$ 0.7	95	0.066, 0.053	High-Y
	12	23.0 $\pm$ 0.4	96	0.075, 0.038	Low-Th, ND
	12	31.0 $\pm$ 0.5	97	0.069, 0.039	Low-Th, ND
	2	26.9 $\pm$ 1.1	96	0.073, 0.043	Low-Th, ND
13	4	27.1 $\pm$ 1.2	97	0.032, 0.066	ND
	1	451 $\pm$ 6	>99	0.043, 0.046	Very high U incl. in Grt
	1	309 $\pm$ 7	>99	0.043, 0.046	Very high U incl. in Grt
20	3	17.4 $\pm$ 0.5	91	0.025, 0.091	Rim, high-Y grain
	3	18.0 $\pm$ 0.4	84	0.060, 0.045	Core, high-Y grain
	1	18.7 $\pm$ 1.0	89	0.059, 0.045	High-Y rim
	1	18.9 $\pm$ 1.8	91	0.028, 0.042	Low-Y core
10	1	13.9 $\pm$ 0.5	89	0.057, 0.033	High-Y
	1	15.0 $\pm$ 0.4	91	0.068, 0.040	High-Y
	1	15.0 $\pm$ 0.3	93	0.069, 0.040	High-Y
	1	15.0 $\pm$ 0.3	93	0.068, 0.040	High-Y
	1	15.2 $\pm$ 0.4	93	0.068, 0.020	High-Y
	1	15.4 $\pm$ 0.3	93	0.057, 0.033	High-Y
	2	14.8 $\pm$ 0.5	91	0.060, 0.046	High-Y
	2	19.5 $\pm$ 1.2	90	0.013, 0.014	Low-Y
6	2	20.0 $\pm$ 0.7	85	0.015, 0.012	Low-Y
	2	20.0 $\pm$ 0.7	85	0.015, 0.012	Low-Y
4	3	13.6 $\pm$ 0.4	90	0.045, 0.036	High-Y rim
	3	14.8 $\pm$ 0.2	89	(mixed)	(mixed)
	3	16.4 $\pm$ 0.3	93	0.012, 0.048	Low-Y core
	5	15.6 $\pm$ 0.6	91	0.013, 0.039	Low-Y core
	5	16.4 $\pm$ 1.2	90	0.032, 0.040	Intermed-Y
	5	16.4 $\pm$ 1.2	90	0.032, 0.040	Intermed-Y
25	2	15.4 $\pm$ 0.7	87	0.043, 0.043	High-Y
	2	16.4 $\pm$ 0.5	91	0.068, 0.040	High-Y
	2	16.4 $\pm$ 0.7	90	0.070, 0.044	High-Y
	2	NA	NA	0.006, 0.053	Low-Y
27	1	14.3 $\pm$ 0.5	87	0.045, 0.049	High-Y rim
	1	14.3 $\pm$ 0.5	88	0.052, 0.048	High-Y rim
	2	22.5 $\pm$ 0.7	92	0.000, 0.057	Low-Y core
	2	25.0 $\pm$ 0.8	93	0.000, 0.060	Low-Y core
31	1	15.3 $\pm$ 1.4	86	0.021, 0.052	High-Y grain
31a	7	20.4 $\pm$ 1.0	89	0.006, 0.091	Low-Y incl. in Grt
	2	21.7 $\pm$ 2.0	69	0.001, 0.058	Low-Y core
	2	22.3 $\pm$ 1.5	83	0.002, 0.068	Low-Y core
74	1	12.8 $\pm$ 1.5	87	0.012, 0.047	High-Y, low-Th rim
	1	25.9 $\pm$ 1.0	94	0.001, 0.059	ND
	2	22.0 $\pm$ 0.6	91	0.000, 0.080	ND
	9a	18.1 $\pm$ 2.3	94	0.009, 0.071	Incl. in Grt
	9b	22.6 $\pm$ 1.1	94	0.020, 0.055	Incl. in Grt
75	7	20.1 $\pm$ 1.1	90	NA	Incl. in Grt
	3	26.1 $\pm$ 2.8	98	0.015, 0.054	ND
	3	29.6 $\pm$ 5.6	98	0.007, 0.050	ND
	12	28.7 $\pm$ 2.4	98	mixed	ND
	10	32.2 $\pm$ 1.0	97	0.037, 0.050	ND
	1	32.4 $\pm$ 0.7	98	0.015, 0.050	ND

Table 3 (continued)

Sample	Grain	Age $\pm 2\sigma$	% radio	$X_Y, X_{Th}$	Comment
75	2	34.4 $\pm$ 0.6	98	0.042, 0.044	ND
	2	36.5 $\pm$ 0.7	98	0.044, 0.048	ND
78	1	14.3 $\pm$ 1.7	73	0.015, 0.053	Incl. in Grt
	3	15.2 $\pm$ 2.0	86	0.032, 0.062	Incl. in Grt core
	3	17.8 $\pm$ 5.0	57	0.033, 0.036	Incl. in Grt core
	4	16.0 $\pm$ 4.5	89	0.000, 0.085	Incl. in Grt core
	4	16.1 $\pm$ 4.8	53	0.000, 0.083	Incl. in Grt core
65	12	10.8 $\pm$ 1.7	75	0.004, 0.040	Low-Y
	15	12.1 $\pm$ 2.4	51	0.007, 0.041	Low-Y incl. in Grt
	3	14.7 $\pm$ 1.0	74	0.009, 0.044	Intermed-Y
62	10	NA	NA	0.029, 0.047	High-Y core
	5	10.4 $\pm$ 0.3	94	0.034, 0.042	ND
	10	10.5 $\pm$ 0.4	88	0.023, 0.059	Low-Y incl. in Grt
	6	11.0 $\pm$ 0.4	93	0.037, 0.024	High-Y
	2	11.4 $\pm$ 1.0	92	0.036, 0.059	High-Y
	3	11.6 $\pm$ 0.5	92	0.039, 0.035	High-Y
40	27	4.0 $\pm$ 0.2	76	0.008, 0.058	ND
	28	4.1 $\pm$ 0.2	63	0.022, 0.041	ND
	14	4.2 $\pm$ 0.2	77	0.018, 0.044	ND
	5	4.4 $\pm$ 0.2	75	0.011, 0.057	Incl. in plagioclase
42	9	2.7 $\pm$ 0.3	67	(All grains have	ND
	12	2.8 $\pm$ 0.2	65	indistinguishable	ND
	11	2.9 $\pm$ 0.8	24	compositions):	ND
	3	3.4 $\pm$ 0.2	75	0.030, 0.050	ND

Various numbers for specific monazite grains reflects the fact that typically several monazite grains were chemically mapped, but only a few were drilled out for microanalysis. Samples 31 and 31a are from the same rock; samples 74 and 75 are from the same outcrop and lithologically indistinguishable. Ages are in Ma and assume a common  $^{208}\text{Pb}/^{204}\text{Pb}$  composition of 38.6. An uncertainty in common  $^{208}\text{Pb}/^{204}\text{Pb}$  of  $\pm 1$  propagates to age uncertainties that are  $\leq 1\%$  for analyses that are  $\geq 70\%$  radiogenic to  $\sim 10\%$  for analyses that are 25% radiogenic, i.e., strongly subordinate to calibration errors for all analyses. NA refers to an important chemical composition that was measured with the electron microprobe to (e.g., to help define “high” vs. “low” Y), but that was not analyzed for Th–Pb age. Comments regarding low- vs. high-Y and low- vs. high-Th reflect internal zoning within individual grains. ND indicates that zoning patterns were non-diagnostic (i.e., distinct low- vs. high-concentration areas were not present). For sample 13, grain 1 is an inclusion in garnet with extremely high U-content and must be out of equilibrium with the rock, as all other (young) monazite grains have concentrations five times lower; this grain is likely either detrital or formed via some low-temperature process (e.g., hydrothermal). For sample 20, monazite 3 is a unique late-stage grain that overprints the fabric; the core has high-Y, nearly identical in composition to the rim of grain 1 from the same rock. The rim of grain 3 has low-Y, likely due to Rayleigh fractionation during growth. All grains are matrix grains unless otherwise noted.

titic rocks high-Y overgrowths reflect melt crystallization and cooling, which in this setting is likely the result of thrusting.

## 5. Monazite ages

In GHS rocks, age probability diagrams from monazite (Fig. 2A,B) delineate the timing of the last growth of prograde subsolidus monazite (youngest low-Y and/or low-Th monazite peak) vs. the timing of final melt crystallization during cooling (high-Y overgrowth). These generally illustrate decreasing ages of metamorphism and high-T structurally downward,

consistent with in-sequence thrusting [1,8]. In the structurally highest rocks (GHS4), near Langtang village, melting and final crystallization of in situ melts must have occurred at  $\sim 20$  and 17–19 Ma, respectively. However, these rocks record older ages, and higher temperatures than structurally lower GHS rocks (GHS1–3), whose monazite ages and chemistry imply latest melting and final crystallization of in situ melts at  $\sim 18$  and 13–16 Ma, respectively. That is, structurally higher rocks were cooling and their melts were crystallizing even as structurally lower rocks were heating and melting. Because of this chronologic difference, we tentatively identify a thrust, here named the Langtang Thrust, between GHS4 and GHS3,

coinciding with the K-feldspar-in isograd. In turn, units GHS3 to GHS1 were cooling and crystallizing even as the next lower structural level (LHS4—Ramgarh Thrust sheet; Fig. 2C) was heating. Although retrograde monazites are not identifiable in LHS4, because the rocks never melted, a muscovite  $^{40}\text{Ar}/^{39}\text{Ar}$  cooling age of  $8.9\pm 0.2$  Ma [19] indicates that the Ramgarh Thrust sheet had cooled through muscovite closure (ca.  $400^\circ\text{C}$  [20]) several Myr before structurally low rocks of the Lesser Himalayan duplex were metamorphosed (3–4 Ma; Fig. 2D).

The monazite ages are generally consistent with previous chronologic summaries in the region [7,8]. However, no previous study investigated monazite chemistry and zoning patterns to this extent. As shown by our data, ages in different monazite grains and domains in a single thrust sheet can span over 20 Myr, with multiple monazite generations, so interpretation of previous data is equivocal. For example, the commonly quoted age of melt crystallization for the GHS of 22 Ma [4,5] may indeed reflect melting in some rocks (e.g., Langtang Thrust sheet), or alternatively fortuitous mixing of different age domains, or inadvertent preferential sampling of a single (but unrepresentative) monazite generation. The monazite and muscovite ages for the Ramgarh Thrust sheet are unusually similar (10.5 vs. 8.9 Ma). To place the muscovite ages in context, in the Langtang area muscovite  $^{40}\text{Ar}/^{39}\text{Ar}$  ages are  $8.5\pm 0.2$  and  $5.5\pm 0.4$  Ma from the base of the MCT, and  $2.3\pm 0.04$  Ma from the Lesser Himalayan duplex [19]. Approximately 10 km to the south, muscovite ages at the GHS–LHS contact are  $8.5\pm 0.2$  and  $9.8\pm 0.4$  [21]. Although in our interpretations below, we prefer a muscovite age for the Ramgarh Thrust Sheet of  $8.9\pm 0.2$  Ma, we do consider the implications of a younger, 5.5 Ma age.

## 6. Thrust rates

The petrologic and chronologic data permit thrusting and convergence rates to be determined provided three simplifying assumptions are met. Our first assumption is that fault slip is equivalent to convergence. This is a good geometric assumption because fault orientations were quite shallow during thrusting [1]. Our second assumption is that the rapid

cooling observed for these mid- to deep-crustal rocks resulted mainly from thrust juxtaposition of a hot hangingwall against a cold footwall, rather than erosion. This is probably also a good assumption, at least for the deeper thrusts. For example, where the Main Himalayan Thrust is at  $\sim 30$  km depth, modern erosion above it is less than 2 mm/yr [22]. Furthermore, observed metamorphic pressures of overlying and underlying plates are not vastly different (Fig. 1, Table 2), implying that vertical exhumation or tectonic denudation could not have been primarily responsible for cooling. However, this assumption cannot be applied to the shallowest and youngest metamorphic rocks of the Lesser Himalayan duplex, because modern erosion rates in that region are extremely high ( $>6$  mm/yr) [22]. Our third assumption for the Langtang and Main Central Thrusts is that only one thrust was active at any time. This assumption may not be accurate, but within the limitations of the data it does provide (maximum) limits on fault slip rates for specific thrusts.

With these assumptions, the minimum amount of cooling ( $\Delta T$ ) during thrusting can be estimated based on the peak temperatures for the thrust sheet of interest and the next lower thrust sheet. Thermal models for the central Himalaya [21,23,24] define temperature–depth distributions near the fault plane, and permit these cooling intervals ( $\Delta T$ 's) to be transformed into thrust distances ( $\Delta d$ 's; Fig. 3). Measured ages of peak metamorphism then provide a maximum duration of this displacement ( $\Delta t$ ), from which each thrusting rate ( $\Delta d/\Delta t$ ) is derived (Table 4). If our third assumption is incorrect (i.e., different faults moved simultaneously), then we would overestimate slip rates for the older thrusts. For example, if the Langtang and Main Central Thrusts moved simultaneously, some of the displacement between them ( $\Delta d$  on the Langtang Thrust) occurred after the MCT sheet started to cool, underestimating  $\Delta t$  and overestimating  $\Delta d/\Delta t$ . Conversely, (a) specific slip rates could have been faster if  $\Delta T$  is underestimated, or occurred over a smaller  $\Delta t$  than assumed, and (b) the slip rate for the Ramgarh Thrust is independent of our third assumption.

The inferred slip rates for the Langtang and Main Central Thrusts are  $\sim 1.5$  and  $\sim 2$  cm/yr between 21 and 11 Ma, similar to the modern 2 cm/yr

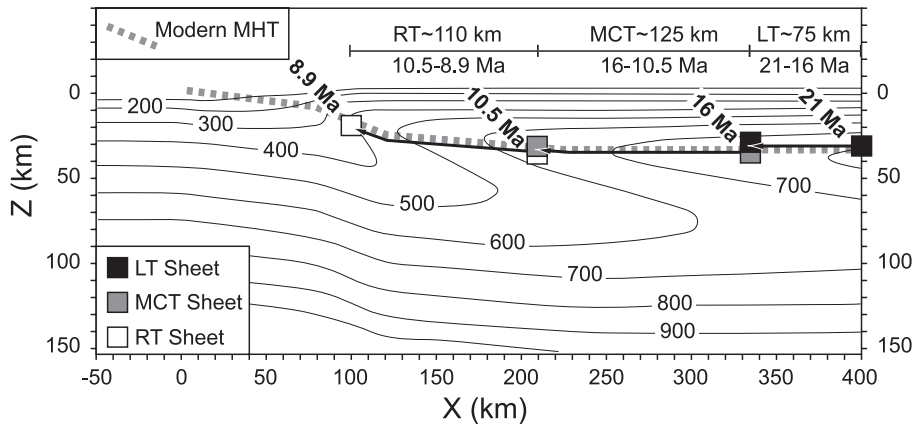


Fig. 3. Schematic illustration of displacements of different thrust packages within the context of the Main Himalayan Thrust (modern MHT) and thermal models for the Himalaya [23]. The timing and location of each point is constrained by  $P$ – $T$  estimates, the age of cooling as determined from monazite or muscovite and the thermal structure.

convergence rate across the Himalaya [2,3]. Because erosion plus slip on lower thrusts could well have affected late-stage cooling for these two thrust sheets, muscovite  $^{40}\text{Ar}/^{39}\text{Ar}$  ages and closure temperatures provide estimates of maximum mean slip rates:  $\sim 2.5$ – $3$  cm/yr. This result strongly supports thermal models that assume  $\sim 2$  cm/yr convergence rates since at least 20 Ma [21,23,24]. Our inferred age of slip for the MCT (16–13 Ma) significantly postdates previous estimates of 22 Ma [4,5], implying either the MCT moved diachronously, or previous age estimates are biased by imperfect characterization of what mineral generation was dated or to which thrust sheet the samples belonged. For the Ramgarh sheet, an estimated transport distance of  $\sim 110$  km is indistinguishable from palinspastic estimates [1] and yields a slip rate of  $\sim 7 \pm 3$  cm/yr, assuming the 8.9 Ma muscovite age.

We do note some difficulty in reconciling the inferred paleoposition of our Ramgarh Thrust samples with the metamorphism of Lesser Himalayan duplex rocks at  $\geq 550$  °C and  $\geq 20$  km depth at 3–4 Ma, at least within the context of the Himalayan thermal models. This problem could reflect model deficiencies (models assume constant convergence rates), or propagation of the ramp towards the foreland. In the latter case, 80 km displacement is more consistent both with the thermal models and the later metamorphism of the Lesser Himalayan duplex rocks, implying a displacement rate for the Ramgarh Thrust of  $\sim 5 \pm 2$  cm/yr. Both the  $7 \pm 3$  and  $5 \pm 2$  cm/yr rates are indistinguishable from the total convergence rate between India and Asia [25], implying that deformation may have briefly partitioned almost exclusively into the Himalaya at  $\sim 10$  Ma. This inference primarily results from the

Table 4

Estimates of thrust temperatures, times, minimum displacements and displacement rates

Thrust	Peak $T$ (°C), $t$ (Ma)	Cooling $T$ (°C), $t$ (Ma)	Distance (km), rate (cm/yr)	Cooling $T$ (°C), $t$ (Ma)	Distance (km), max rate (cm/yr)
Langtang	825, $21 \pm 2$	$\leq 750$ , $16 \pm 1$	80, $1.5 \pm 0.9$	400, $10.5 \pm 1.5$	300, $\leq 3 \pm 0.7$
Main Central	750, $16 \pm 1$	$\leq 625$ , $10.5 \pm 0.5$	120, $2.2 \pm 0.7$	400, $7 \pm 0.1$	225, $\leq 2.5 \pm 0.4$
Ramgarh	625, $\leq 10.5 \pm 0.5$	400, $8.9 \pm 0.1$	110, $7 \pm 3$		

Each temperature estimate has an uncertainty of  $\pm 25$  °C, yielding an uncertainty in the estimated transport distance of  $\sim \pm 30$  km. Estimated transport distances are based on thermal models, but for the Main Central and Ramgarh Thrusts are also almost identical with palinspastic reconstructions [1]. A younger age for muscovite from the Ramgarh Thrust sheet of 5–6 Ma would yield a convergence rate of  $\sim 2$  cm/yr. Ranges in convergence rates are based on propagated uncertainties ( $\pm 2\sigma$ ) in distance and age.

similarity of monazite and muscovite ages. A slower  $\sim 2$  cm/yr rate would require muscovite ages of 5–6 Ma, which is consistent with one muscovite age at the base of the MCT, but not with several others, including those from the same structural level.

Possible rapid movement of the Ramgarh Thrust at ca. 10 Ma is particularly interesting for several reasons. First, there is a pronounced increase in foreland and marine sediment deposition rates at that time [26], which has been proposed to result from collapse of overthickened Tibetan crust and rapid extrusion of the Himalaya [27]. Second, rapid but brief thrusting is consistent with pressure–temperature paths from zoned garnets of the Lesser Himalayan duplex, which are best explained by rapid loading prior to 7–8 Ma followed by either slower convergence or stasis for a few million years, permitting relaxation of isotherms [7, 28]. Third, rocks from at least one major strike-slip fault in Tibet, the Karakoram fault, appear to have experienced a hiatus in their cooling at  $\sim 10$  Ma [29], perhaps implying that deformation was temporarily taken up elsewhere.

With respect to convergence and fault displacement in general, it seems unlikely that the Langtang and Main Central Thrusts moved simultaneously (at lower temperatures) with the Ramgarh, as this would increase the estimated convergence rate above the total for India and Asia at this time [25]. It is possible that the Langtang and Main Central Thrusts moved at similar rates as the Ramgarh, but over shorter time intervals than we estimated. This hypothesis may be tested either through more detailed studies in the GHS, or in transects where GHS-LHS metamorphic disparities are greater, e.g., western Nepal or Bhutan. Whereas our data are generally consistent with a 2–3 cm/yr convergence rate across the Himalaya since  $\sim 20$  Ma (specifically, 300 km of shortening in 12 Myr; Table 4), rates could have varied substantially over Myr intervals. Considering the Himalaya absorb a significant proportion of Indo–Asian strain, this implies that other components in the overall orogen (e.g., Tibet, southeast Asia, etc.) may also exhibit variable strain rates on Myr timescales. Indeed this hypothesis is consistent with the possibility that movement on the Karakoram fault temporarily shut down at  $\sim 10$  Ma [29] via preferential strain partitioning into the

Himalaya. Chemical zoning patterns from LHS garnets further suggest variable strain rates for faults in the Lesser Himalayan duplex on timescales of ca. 25 kyr [30], approaching the kyr timescales for strain rate variations in strike slip systems inferred from comparison of GPS with exposure dating of fault scarps [31] and from paleoseismological trenching of active faults [32].

## 7. Conclusions

Overall, our data lead us to several conclusions. First, monazite ages are correlated with composition, so interpretation of ages requires simultaneous characterization and interpretation of monazite chemistry (e.g., [16,17]). Second, there is a systematic decrease in the age of metamorphism and deformation structurally downward, indicating simple in-sequence thrusting [1,8]. Third, the average convergence rate over the Himalaya as inferred petrologically is consistently ca. 2 cm/yr since ca. 22 Ma. Fourth, convergence rates in the Himalaya could have varied by a factor of 2–3. Finally, and more generally, major fault systems appear to exhibit strain rate variability on timescales of Myr (this study, [29]), tens of kyr [30] and kyr [31,32].

## Acknowledgements

We thank G. Gehrels and M. Hubbard for their reviews, which improved the clarity of the manuscript, M. Grove and A. Schmitt for their help with the ion probe, and T. Ojha for field support. This material is based upon work supported by the National Science Foundation under Grant No. EAR 0073803 to MJK.

## References

- [1] P.G. DeCelles, D.M. Robinson, J. Quade, T.P. Ojha, C.N. Garzione, P. Copeland, B.N. Upreti, Stratigraphy, structure, and tectonic evolution of the Himalayan fold-thrust belt in western Nepal, *Tectonics* 20 (2001) 487–509.
- [2] R. Bilham, K. Larson, J. Freymueller, Indo–Asian convergence rates in the Nepal Himalaya, *Nature* 311 (1997) 621–626.
- [3] K.M. Larson, R. Bürgmann, R. Bilham, J.T. Freymueller, Kinematics of the India–Eurasia collision zone from GPS measurements, *J. Geophys. Res.* 104 (1999) 1077–1093.

- [4] K.V. Hodges, R.R. Parrish, M.P. Searle, Tectonic evolution of the central Annapurna Range, Nepalese Himalayas, *Tectonics* 15 (6) (1996) 1264–1291.
- [5] M.R.W. Johnson, G.J.H. Oliver, R.R. Parrish, S.P. Johnson, Synthrusting metamorphism, cooling, and erosion of the Himalayan Kathmandu Complex, Nepal, *Tectonics* 20 (2001) 394–415.
- [6] T.M. Harrison, F.J. Ryerson, P. Le Fort, A. Yin, O.M. Lovera, E.J. Catlos, A late Miocene–Pliocene origin for the central Himalayan inverted metamorphism, *Earth Planet. Sci. Lett.* 146 (1997) E1–E7.
- [7] E. Catlos, T.M. Harrison, M.J. Kohn, M. Grove, O.M. Lovera, F.J. Ryerson, B.N. Upreti, Geochronologic and thermobarometric constraints on the evolution of the Main Central Thrust, central Nepal Himalaya, *J. Geophys. Res.* 106 (2001) 16177–16203.
- [8] D.M. Robinson, P.G. DeCelles, C.N. Garzzone, O.N. Pearson, T.M. Harrison, E.J. Catlos, Kinematic model for the Main Central Thrust in Nepal, *Geology* 31 (2003) 359–362.
- [9] S. Inger, N.B.W. Harris, Tectonothermal evolution of the High Himalayan crystalline sequence, Langtang Valley, northern Nepal, *J. Metamorph. Geol.* 10 (1992) 439–452.
- [10] A.M. Macfarlane, K.V. Hodges, D. Lux, A structural analysis of the Main Central Thrust zone, Langtang National Park, central Nepal Himalaya, *Geol. Soc. Am. Bull.* 104 (1992) 1389–1402.
- [11] A.M. Macfarlane, An evaluation of the inverted metamorphic gradient at Langtang National Park, central Nepal Himalaya, *J. Metamorph. Geol.* 13 (1995) 595–612.
- [12] O.N. Pearson, Structural evolution of the central Nepal fold-thrust belt and regional tectonic and structural significance of the Ramgarh thrust, Ph.D., University of Arizona, 2002.
- [13] T.M. Harrison, K.D. McKeegan, P. LeFort, Detection of inherited monazite in the Manaslu leucogranite by  $^{208}\text{Pb}/^{232}\text{Th}$  ion microprobe dating: crystallization age and tectonic significance, *Earth Planet. Sci. Lett.* 133 (1995) 271–282.
- [14] J.S. Stacey, J.D. Kramers, Approximation of terrestrial lead isotope evolution by a two-stage model, *Earth Planet. Sci. Lett.* 26 (2) (1975) 207–221.
- [15] R.R. Parrish, U–Pb dating of monazite and its application to geological problems, *Can. J. Earth Sci.* 27 (1990) 1431–1450.
- [16] F.S. Spear, J.M. Pyle, Apatite, monazite and xenotime in metamorphic rocks, *Rev. Mineral. Geochem.* 48 (2002) 293–335.
- [17] J.M. Pyle, F.S. Spear, Four generations of accessory-phase growth in low-pressure migmatites from SW New Hampshire, *Am. Mineral.* 88 (2003) 338–351.
- [18] M.J. Kohn, M.A. Malloy, Formation of monazite via prograde metamorphic reactions among common silicates: implications for age determinations, *Geochim. Cosmochim. Acta* 68 (2004) 101–113.
- [19] A.M. Macfarlane, Chronology of tectonic events in the crystalline core of the Himalaya, Langtang National Park, central Nepal, *Tectonics* 12 (4) (1993) 1004–1025.
- [20] I. McDougall, T.M. Harrison, *Geochronology and thermochronology by the  $^{40}\text{Ar}/^{39}\text{Ar}$  method*, Oxford University Press, Oxford, 1999, 269 pp.
- [21] P. Copeland, P. LeFort, P. Henry, S.M. Raï, D. Foster, R.R. Parrish, A. Pecher, K. Stüwe, B.N. Upreti, A. Raza, Neogene tectonothermal development of the Himalayan thrust system in the Kathmandu region, Nepal, *Geol. Soc. Am. Bull.*, in review.
- [22] J. Lavé, J.P. Avouac, Fluvial incision and tectonic uplift across the Himalayas of central Nepal, *J. Geophys. Res.* 106 (2001) 26561–26591.
- [23] P. Henry, X. LePichon, B. Goffé, Kinematic, thermal and petrological model of the Himalayas: constraints related to metamorphism within the underthrust Indian crust and topographic evolution, *Tectonophysics* 273 (1997) 31–56.
- [24] A.D. Huerta, L.H. Royden, K.V. Hodges, The effects of accretion, erosion and radiogenic heat on the metamorphic evolution of collisional orogens, *J. Metamorph. Geol.* 17 (1999) 349–366.
- [25] C.T. Klootwijk, J.S. Gee, J.W. Peirce, G.M. Smith, P.L. McFadden, An early India–Asia contact; paleomagnetic constraints from Ninetyeast Ridge, ODP Leg 121, *Geology* 20 (1992) 395–398.
- [26] D.W. Burbank, R.A. Beck, T. Mulder, The Himalayan foreland basin, in: A. Yin, T.M. Harrison (Eds.), *The tectonics of Asia*, Cambridge University Press, New York, 1996, pp. 205–226.
- [27] P. Huyghe, A. Galy, J.-L. Mugnier, C. France-Lanord, Propagation of the thrust system and erosion in the Lesser Himalaya: geochemical and sedimentological evidence, *Geology* 29 (2001) 1007–1010.
- [28] M.J. Kohn, E.J. Catlos, F.J. Ryerson, T.M. Harrison, Pressure–temperature–time path discontinuity in the Main Central Thrust zone, central Nepal, *Geology* 29 (2001) 571–574.
- [29] W.J. Dunlap, R.F. Weinberg, M.P. Searle, Karakoram fault zone rocks cool in two phases, *J. Geol. Soc. (London)* 155 (1998) 903–912.
- [30] M.J. Kohn, Oscillatory- and sector-zoned garnets record cyclic (?) rapid thrusting in central Nepal, *Geochem. Geophys. Geosyst.* (2004), in press.
- [31] J. van der Woerd, P. Tapponnier, F.J. Ryerson, A.S. Meriaux, B. Meyer, Y. Gaudemer, R.C. Finkel, M.W. Caffee, Z. Guoguang, X. Zhiqin, Uniform postglacial slip-rate along the central 600 km of the Kunlun Fault (Tibet), from  $^{26}\text{Al}$ ,  $^{10}\text{Be}$ ,  $^{14}\text{C}$  dating of riser offsets, and climatic origin of the regional morphology, *Geophys. J. Int.* 148 (2002) 356–388.
- [32] R. Weldon, K. Scharer, T. Fumal, G. Biasi, Wrightwood and the earthquake cycle: what a long recurrence record tells us about how faults work, *GSA Today* 14 (2004) 4–10.
- [33] P. Le Fort, Himalayas; the collided range; present knowledge of the continental arc, *Am. J. Sci.* 275-A (1975) 1–44.
- [34] J.M. Ferry, F.S. Spear, Experimental calibration of the partitioning of Fe and Mg between biotite and garnet, *Contrib. Mineral. Petrol.* 66 (1978) 113–117.
- [35] R.G. Berman, Mixing properties of Ca–Mg–Fe–Mn garnets, *Am. Mineral.* 75 (1990) 328–344.
- [36] M.J. Holdaway, B. Mukhopadhyay, M.D. Dyar, C.V. Guidotti, B.L. Dutrow, Garnet–biotite geothermometry revised: new Margules parameters and a natural specimen data set from Maine, *Am. Mineral.* 82 (1997) 582–595.

- [37] T.D. Hoisch, Empirical calibration of six geobarometers for the mineral assemblage quartz+muscovite+biotite+plagioclase+garnet, *Contrib. Mineral. Petrol.* 104 (2) (1990) 225–234.
- [38] A.M. Koziol, Recalibration of the garnet–plagioclase– $\text{Al}_2\text{SiO}_5$ –quartz (GASP) geobarometer and application to natural parageneses, *EOS Trans. Am. Geophys. Union* 70 (1989) 493.
- [39] F.S. Spear, J.T. Cheney, A petrogenetic grid for pelitic schists in the system  $\text{SiO}_2$ – $\text{Al}_2\text{O}_3$ –FeO–MgO– $\text{K}_2\text{O}$ – $\text{H}_2\text{O}$ , *Contrib. Mineral. Petrol.* 101 (1989) 149–164.
- [40] F.S. Spear, M.J. Kohn, J.T. Cheney, P–T paths from anatectic pelites, *Contrib. Mineral. Petrol.* 134 (1) (1999) 17–32.